

**NICST Internal Memo**

Date: January 3, 2011  
From: Jeff McIntire and Sanxiong Xiong  
To: Bruce Guenther, Jim Butler, and Jack Xiong  
Subject: Analysis of the Radiometric Calibration from VIIRS F1 RC-05 Part 1 Test  
(Nominal Plateau, Electronic Side B)

---

References:

- [1] 'Sensor Performance Verification Plan,' PVP154640-101.
- [2] 'Performance Specification Sensor Specification,' ps154640-101c.
- [3] NICST\_REPORT\_10\_069, 'Emissive Band Radiometric Calibration: FU1 RC-05 Part 1 Nominal Plateau (B side),' Jeff McIntire, July 9, 2010.
- [4] Y18352, 'Performance Verification Review: Thermal Emissive Band Radiometric Response Characterization (RC-3 and RC-5 Tests),' Eric Johnson and Jim Young, January 18, 2006.
- [5] IT\_OBCBB\_EDU\_Temp\_081112, 'OBC Blackbody Temperature Calculation,' Courtney Ranshaw, November 11, 2008.
- [6] F1\_RSR\_PVR\_JT\_091412, 'Performance Verification Report – VIIRS Relative Spectral Response (PVP Section 4.6),' Justin Trice, Nicholas Lardas, and Mark Bliton, December 4, 2009.
- [7] Y24182, 'VIIRS FU1 Test Analysis Report fro FP-10 Part 1, Reflective Band Response vs Scan Angle (Version 2),' Courtney Ranshaw, February 19, 2008.
- [8] Y22061, 'VIIRS Test Analysis Report for RC-05, Part 1,' Courtney Ranshaw and Mina Mitani, January 26, 2007.
- [9] RDW\_VIIRS-W070B, 'Flight 1 Wavier for Emissive Band Radiometry Requirement SRV0448,' Laura Kneller and Joe Essner, September 10, 2009.

**1. Introduction**

The VIIRS F1 thermal vacuum test RC-05 Part 1 was designed to examine the sensor response to well calibrated, external sources [the Blackbody Calibration Source (BCS) and the Three Mirror Collimator (TMC) blackbody] in a near space-like environment. This test consisted of two sections: low and high temperature. The low temperature portion was conducted at a series of discrete temperature levels for the BCS and TMC designed at access the full dynamic range of the single gain bands and M13 high gain. The high temperature segment was designed to calibrate the low gain sector of M13 using the TMC blackbody.

This work will focus on the radiometric gains and sensitivity as well as on compliance with a number of specifications from the RC-05 test at Nominal plateau, electronic side B [1,2]. A preliminary investigation of this test was reported in [3].

Tables 1 and 2 list the relevant UAIDs, collects, and gain mode as well as the BCS, TMC, and OBC temperatures. The TMC and BCS sources were located in the middle and last collect windows (or scan angles of -7.5 and 40.2 degrees). In addition, the Space View Source (SVS) was positioned in the Space View (SV) port.

The VIIRS sensor was operated in diagnostic mode and each collect contains 100 scans. The sensor was set to fixed high gain for the low temperature portion; all three gain modes were used for the high temperature sequence (although only fixed low gain is used in this work). The general outline of the methodology used in this work follows from [1,4] with some modifications.

## 2. Data Processing

The BCS data analyzed here is restricted to a subset of the Earth View (EV) samples in a given collect for which the BCS or TMC source yielded a stable response. The following sample ranges were used in this work: samples 1060 – 1319 for M bands and samples 2120 – 2639 for I bands when using the BCS source and samples 610 – 659 for the M bands and samples 1220 – 1319 for the I bands when using the TMC source. All the samples for both the On Board Calibrator (OBC) blackbody and SV were analyzed.

The DN for the EV sector is truncated to 12 bits while the calibration sectors report DN in 14 bits. This leads to a bias in the dn. As a result, all calibration view data used in this work was truncated to 12 bits.

The response was analyzed using the scan method. First, the  $DN_{SV}$  was averaged over all samples in a given scan. Then, the sample averaged  $DN_{SV}$  was subtracted from each sample of the  $DN_{EV}$  in the corresponding scan to produce the dn. Next, the dn was averaged over samples and the standard deviation of all samples for a specific scan was calculated. Note that the Half Angle Mirror (HAM) sides alternate from scan to scan such that there are 50 scans for each HAM side. Additionally, the I band data is divided into two subsamples; the larger for both SV and OBC is always matched to the larger for the EV, to ensure the proper background subtraction. Lastly, the dn and standard deviation are averaged over scans (each HAM side separately). The same treatment was used on the OBC data to produce the  $dn_{OBC}$ .

The temperatures ( $T_{xxx}$ ) of the following were extracted: BCS, OBC, TMC, TMC optics, SVS, HAM, Rotating Telescope Assembly (RTA), scan CAVity (CAV), and OBC blackbody SHield (SH). The OBC, HAM, CAV, and SH temperatures were acquired using the LRV telemetry extractor while the BCS, TMC, TMC optics, and SVS temperatures were obtained from the Ground Support Equipment (GSE) files. The RTA temperature is the CAV temperature minus 8 degrees K.

Six thermistors within the OBC are used to track the OBC temperature. In addition, three calibration resistors in the back of the OBC are used to correct for self heating effects in the six main thermistors [5].

## 2.1 Radiometric Calibration – Single Gain and M13 High Gain

In this section, the calibration of the single gain bands and M13 high gain are considered. The discussion of the M13 low gain calibration using the TMC blackbody will be discussed in a later section.

For each of the extracted temperatures, the Planck radiance at a given wavelength is calculated from

$$L_{xxx}(C, \lambda, T_{xxx}(C)) = \frac{2hc}{\lambda^5} \frac{1}{e^{hc/\lambda kT_{xxx}} - 1} \quad (1)$$

where C refers to collect. The radiance for a particular band and detector is determined by weighting the Planck radiance by the Relative Spectral Response (RSR) over the In Band (IB) region (between the 1% response points), or

$$\langle L_{xxx}(C, B, D) \rangle = \frac{\int_{IB} RSR(B, D, \lambda) L_{xxx}(C, \lambda, T_{xxx}) d\lambda}{\int_{IB} RSR(B, D, \lambda) d\lambda}, \quad (2)$$

where B and D represent band and detector, respectively. The RSR used here was provided by the Raytheon [6]. Because the external source temperatures are not recorded on a scan basis, their radiances are determined on a collect basis. In contrast, the internal source temperatures are recorded on a scan basis. However, the scan dependence is only retained when determining the OBC at-detector radiance.

The effective OBC radiance is

$$\begin{aligned} \langle L_{OBC}(C, B, D, j_H) \rangle_{eff} &= \varepsilon_{OBC}(B) \langle L_{OBC}(C, B, D, j_H) \rangle \\ &\quad - [1 - \varepsilon_{OBC}(B)] [F_{CAV} \langle L_{CAV}(C, B, D, j_H) \rangle \\ &\quad + F_{SH} \langle L_{SH}(C, B, D, j_H) \rangle + F_{RTA} \langle L_{RTA}(C, B, D, j_H) \rangle] \end{aligned} \quad (3)$$

where  $\varepsilon_{OBC}$  is the emissivity of the OBC and  $j_H$  represents the scan number (HAM side dependent).  $F_{CAV}$ ,  $F_{SH}$ , and  $F_{RTA}$  are the shape factors related to the solid angles of the CAV, SH, and RTA as viewed by the OBC; these factors determine the reflectance off the OBC.

The background radiance contributions from the RTA, HAM, and SVS are defined as

$$\begin{aligned} \langle L_{Bkg-yyy}(C, B, H, D) \rangle &= r_{VS}(B, H, D, \phi_{SVS}) \langle L_{SVS}(C, B, D) \rangle \\ &\quad - \frac{[r_{VS}(B, H, D, \phi_{SVS}) - r_{VS}(B, H, D, \phi_{yyy})]}{\rho_{RTA}(B)} \\ &\quad \times [\langle L_{HAM}(C, B, D) \rangle - (1 - \rho_{RTA}(B)) \langle L_{RTA}(C, B, D) \rangle] \end{aligned} \quad (4)$$

The yyy refers to either the BCS or OBC, depending on which source is being considered. In addition, the radiances are corrected for Response Versus Scan (RVS) angle and the reflectance factor of the RTA optics ( $\rho_{RTA}$ ). Note that  $\phi_{yyy}$  refers to the HAM angle of incidence for the BCS or OBC source (the RVS is normalized to 1.0 at the OBC HAM angle). The RVS used in this work was provided by Raytheon [7]. The HAM

and RTA contributions to the background radiance retain their scan dependence when used in the background for the at-detector OBC radiance.

Now the background subtracted, at-detector source radiances are determined by

$$\Delta L_{OBC}(C, B, D, j_H) = \langle L_{OBC}(C, B, D, j_H) \rangle_{eff} - \langle L_{Bkg-OBC}(C, B, D, j_H) \rangle, \quad (5)$$

and

$$\Delta L_{BCS}(C, B, H, D) = rvs(B, H, D, \phi_{BCS}) \langle L_{BCS}(C, B, D) \rangle - \langle L_{Bkg-BCS}(C, B, H, D) \rangle. \quad (6)$$

The background subtracted radiance is modeled by a polynomial in the detector response. These polynomials take the form

$$\Delta L_{BCS}(C, B, H, D) = GC(C, B, H, D, S) \sum_{i=0}^N a_i^{BCS}(B, H, D, S) dn_{BCS}^i(C, B, H, D, S). \quad (7)$$

Least-squares fits were performed over the dynamic range at the linear, quadratic, and cubic levels (or order N) to determine the polynomial coefficients. Data for which the SNR was below 1.0 was excluded from the fitting. The inverse of the linear term ( $1/a_1$ ) is the radiometric gain (detector responsivity). The Gain Correction (GC) is an additional factor designed to compensate for any drift in the linear gain that might occur over the timescale of the RC-05 test and is defined as

$$GC(C, B, H, D, S) = \frac{\Delta L_{OBC}(C_{close}, B, D) \sum_{i=0}^N a_i^{BCS}(B, H, D, S) dn_{OBC}^i(C, B, H, D, S)}{\Delta L_{OBC}(C, B, D) \sum_{i=0}^N a_i^{BCS}(B, H, D, S) dn_{OBC}^i(C_{close}, B, H, D, S)}. \quad (8)$$

where  $C_{close}$  is the collect at which the BCS and OBC temperatures are closest. The GC is initially set equal to 1.0; the BCS coefficients are then determined using Eq. (7). Next, the GC is calculated and the process is repeated until the GC converges. The scan average value of GC is used in this work.

Lastly, the retrieved calibration source radiance is defined as

$$\begin{aligned} \langle L_{BCS}(C, B, D, S, j_H) \rangle_{ret} &= \frac{\Delta L_{OBC}(C, B, D, j_H) \sum_{i=0}^N a_i^{BCS}(B, H, D, S) dn_{BCS}^i(C, B, H, D, S)}{rvs_{BCS}(B, H, D, \phi_{BCS}) \sum_{i=0}^N a_i^{BCS}(B, H, D, S) dn_{OBC}^i(C, B, D, S, j_H)} \\ &\quad + \langle L_{Bkg-BCS}(C, B, H, D) \rangle \end{aligned} \quad (9)$$

The retrieved radiance is then averaged over scans. The ratio of the at-detector OBC radiance to the polynomial in OBC dn is a scan by scan correction for linear drift in the coefficients that will be applied on orbit.

## 2.2 Radiometric Calibration – M13 Low Gain

The low gain radiometric calibration for M13 was measured separately from the high gain and all the thermal single gain bands. The BCS source has a maximum temperature

of 345 K, which is at the very low end of the M13 low gain dynamic range. As a result, the TMC blackbody is used to access the high temperature region. The TMC radiance is modeled as

$$\begin{aligned} \Delta L_{TMC}(C, B, H, D) = & rvs(B, H, D, \phi_{TMC}) \{ \varepsilon_{TMC}(B) \langle L_{TMC}(C, B, D) \rangle \\ & + (1 - \tau_{TMC}) \langle L_{TMC-optics}(C, B, D) \rangle + (1 - \rho_{window}) \langle L_{window}(C, B, D) \rangle \}, \\ & - \langle L_{Bkg-TMC}(C, B, H, D) \rangle \end{aligned} \quad (10)$$

where the background radiance is determined as in Eq. (4). The TMC emissivity was supplied by the vendor, and is given by

$$\varepsilon_{TMC}(C) = 0.415[d_0 + d_1 T_{TMC}(C)], \quad (11)$$

where the  $d_0$  and  $d_1$  are determined from a linear fit of [0.94,1.0,1.01] and [303,473,733]. The radiance from the TMC optics was determined from a thermistor placed nearby and the radiance from the vacuum chamber window was calculated using the plateau temperature (the window reflectance used was 0.71). The transmission of the TMC optics is unknown. To determine the transmission, the TMC must be cross-calibrated to the BCS in the low temperature region (below 345 K).

The cross-calibration is accomplished by assuming that

$$\Delta L_{TMC}(C, B, H, D) = \sum_{i=0}^N a_i^{BCS}(B, H, D, S) dn_{TMC}^i(C, B, H, D, S).. \quad (11)$$

and then solving Eq. (10) for the TMC optics transmission using low temperature data. This transmission is applied to the high temperature collects in fixed low gain, through Eq. (10). Then, the calculated high temperature radiance is related to the dn by the following:

$$\Delta L_{TMC}(C, B, H, D) = \sum_{i=0}^N a_i^{TMC}(B, H, D, S) dn_{TMC}^i(C, B, H, D, S). \quad (12)$$

The coefficients are determined though least-squares fitting. Lastly, the retrieved calibration source radiance is defined as

$$\begin{aligned} \langle L_{TMC}(C, B, H, D, S) \rangle_{ret} = & \frac{\sum_{i=0}^N a_i^{TMC}(B, H, D, S) dn_{TMC}^i(C, B, H, D, S)}{rvs_{TMC}(B, H, D, \phi_{TMC})} \\ & + \langle L_{Bkg-TMC}(C, B, H, D) \rangle \end{aligned} \quad (13)$$

As on-orbit the scan by scan correction is not used for M13 low gain, it is not used here (for an OBC temperature of 292 K, M13 low gain dn is approximately 4).

### 2.3 Radiometric Sensitivity

The Signal to Noise Ratio (SNR) is calculated as the ratio of the dn to the standard deviation. This calculation was preformed using the following three methods:

$$SNR_{sample}(C, B, H, D, S) = \frac{1}{M} \sum_{i=0}^{M-1} \frac{dn_{scan}(C, B, H, D, S, i)}{\sigma_{scan}(C, B, H, D, S, i)}, \quad (14)$$

$$SNR_{scan}(C, B, H, D, S) = \frac{1}{P} \sum_{j=0}^{P-1} \frac{dn_{sample}(C, B, H, D, S, j)}{\sigma_{sample}(C, B, H, D, S, j)}, \quad (15)$$

and

$$SNR_{overall}(C, B, H, D, S) = \frac{dn_{overall}(C, B, H, D, S)}{\sigma_{overall}(C, B, H, D, S)}, \quad (16)$$

where the sums are over all extracted samples (M) in a scan and over all extracted scans (P). Eq. (14) describes the sample method, where the SNR is determined over all scans at each sample and then averaged over all extracted samples. Eq. (15) describes the scan method, where the SNR is determined over all extracted samples at each scan and then averaged over all scans. Eq. (16) describes the overall method, where the SNR is determined over all scans and samples simultaneously. The SNR used in this work is the largest of the three (which should be closest to the true sensor SNR).

Next, the SNR is modeled using the following function:

$$\begin{aligned} SNR(C, B, H, D, S) = & \langle L_{BCS}(C, B, H, D, S) \rangle_{ret} [b_0(B, H, D, S) \\ & + b_1(B, H, D, S) \langle L_{BCS}(C, B, H, D, S) \rangle_{ret} \\ & + b_2(B, H, D, S) \langle L_{BCS}(C, B, H, D, S) \rangle_{ret}^2]^{1/2}. \end{aligned} \quad (17)$$

The coefficients (b<sub>i</sub>) are determined by fitting this function to the data within the specified dynamic range. Eq. (17) is then used to evaluate the SNR at L<sub>TYP</sub>.

The Noise Equivalent delta Temperature (NEdT) is the fluctuation in the scene temperature that is equivalent to the system noise; the NEdT is computed via the equation

$$NEdT(C, B, D, H, S) = \frac{NEdL(C, B, H, D, S)}{\frac{\partial L(B, T)}{\partial T}} = \frac{\langle L_{BCS}(C, B, H, D, S) \rangle_{ret}}{SNR(C, B, H, D, S) \frac{\partial L(B, T)}{\partial T}}. \quad (18)$$

The derivative is of the Planck radiance with respect to the temperature evaluated at T<sub>TYP</sub>. This NEdT is also determined at L<sub>TYP</sub> using Eq. (17), in order to compare with the specification SRV0053 (listed in Table 4).

## 2.4 Specifications

The six specifications that are considered in this memo are listed in Table 3 [2].

SRV0448 investigates the response characterization, which is essentially a measure of the goodness of fit. This requirement is accessed using the Radiometric Response Characterization Uncertainty (RRCU), or

$$RRCU(B, H, D, S) = \sqrt{mean_C [\Delta_{fit}(C, B, H, D, S)]^2 + \sigma_C [\Delta_{fit}(C, B, H, D, S)]^2}. \quad (19)$$

This specification is met if the RRCU is less than 0.1 %. Here Δ<sub>fit</sub> is the fractional fitting residual derived from a polynomial fit of ΔL<sub>BCS</sub> versus dn, as defined in Eq. (7).

The specification SRV0595 evaluates the response linearity. In this work, SRV0595 is investigated using the Relative Response Non-Linearity (RRNL), or

$$RRNL(B, H, D, S) = \frac{\max_C \left( \left| \Delta_{fit}(C, B, H, D, S) \Delta L_{BCS}(C, B, H, D) \right| \right)}{L_{MAX}(B)}. \quad (20)$$

As this is a measurement of the deviation from linearity, the fitting residual (not the fractional residual) for a linear polynomial fit is used to calculate the RRNL. The VIIRS sensor meets this requirement if the RRNL is less than 1 %.

The absolute calibration uncertainty is addressed by the following two requirements: SRV0545 and SRV0546. The absolute calibration uncertainty includes all the uncertainties associated with the calibration. This is beyond the scope of this work; however, the fit uncertainty contribution to the absolute uncertainty can be analyzed using the Absolute Radiance Difference (ARD), or

$$ARD(C, B, H, D, S) = 100 \frac{\langle L_{BCS}(C, B, H, D, S) \rangle_{ret} - \langle L_{BCS}(C, B, D) \rangle}{\langle L_{BCS}(C, B, D) \rangle}. \quad (21)$$

This is just the percent difference between the retrieved and RSR corrected Planck radiances (essentially, the ARD is a measure of fit uncertainty's effect on the accuracy of the retrieved radiance). This requirement is compared against the values listed in Table 5 for the specified scene temperatures. These requirements are compared to the ARD at the BCS temperature nearest to the specified scene temperatures.

The final specification (SRV0613) considered here investigates the detector to detector uniformity (or striping). This particular requirement is assessed by means of the Relative Response Uniformity (RRU), or

$$RRU(C, B, H, D, S) = \max_D \left( \left| \langle L_{BCS}(C, B, H, D, S) \rangle_{ret} - \langle L_{BCS}(C, B, D) \rangle - \left( \langle L_{BCS}(C, B, H, D, S) \rangle_{ret} - \langle L_{BCS}(C, B, D) \rangle \right) / NEDL(C, B, H, D, S) \right| \right) \quad (22)$$

where the difference between the retrieved radiance and the RSR corrected source radiance is used here. This delta radiance was employed in place of the RSR corrected radiance to avoid any possible spectral variation from detector to detector produced in the RSR by the spectral smile of the SpMA [8]. Also, note that the measured NEDL is used to compute the RRU. This specification is met if the RRU is less than 1.0.

### 3. Analysis

#### 3.1 Radiometry

The sensor specification defines the dynamic range over which VIIRS thermal bands must be calibrated. However, valid science data may exist for some bands outside the specified range. In this work the dynamic range was optimized to include all available data not contaminated at high temperature by saturation and for which the SNR was greater than one at low temperature. The specified and optimized dynamic ranges are listed in Table 6. The dynamic ranges are also shown in Figure 1; the blue lines indicate the specified dynamic range, the black lines represent the optimized dynamic range, and the red lines indicate the scene temperatures where the SNR is equal to one [determined

from Eq. (17)] and the saturation temperature. The saturation calculation will be described in a later work. Note that the maximum BCS temperature is 345 K and as such was a limiting factor on the extension of the dynamic range. In addition, the SNR fell below one inside the specified dynamic range for I4 and M14. The minimum measured BCS temperature of 190 K was a limiting factor on the extension of the dynamic range for most LWIR bands. For M13 low gain, the optimized range corresponded to the retrieved scene temperature range measured.

The thermal bands, fit using a quadratic polynomial, are shown in Figure 2 for all high gain bands and all detectors. Data with SNR less than 1.0 was excluded; this occurred only for band I4 at 210 K and M14 at 190 K. Note that detector 1 in band M12 is Out Of Family (OOF). The radiance residual for each high gain band is shown in Figure 3. The residual is generally small for the LWIR bands I5 and M14 – M16 (less than 1.0 %). The residuals for I4, M12, and M13 in particular increase at lower temperatures (up to 10% at  $T_{MIN}$ ); these bands are known to exhibit greater nonlinearity at low radiances. Although only HAM side A was shown, HAM sides A and B yield very similar results.

The median high gain calibration coefficients for a quadratic polynomial fit are given in Table 7. In addition, the median gains ( $1/a_1$ ) are listed in Table 8. Note that the offset term ( $a_0$ ) is generally small (on the order of  $10^{-2}$  or less); this indicates that the model is generally consistent with an offset of zero. However, the added degree of freedom is useful in constraining the data, so setting  $a_0 = 0$  is not endorsed here. The nonlinear term is also very small (on the order of  $10^{-8}$  or less), which indicates that the instrument has a very linear response to the input radiance. Notice that the nonlinear term is negative for all the MWIR bands and positive for all the LWIR bands; thus the curvature of the fit is opposite from the MWIR to LWIR bands. The linear term ( $a_1$ ) is dominant for the thermal bands. The calibration coefficients are plotted versus detector for all high gain bands in Figures 4 – 6. Note that the HAM sides are generally very consistent. In addition, there is some odd – even dependence in the gain for bands I5, M12, and M13. Also, the gains tend to decrease with detector number for the LWIR bands (I5, M14 – M16). As mentioned before, M12 detector 1 is OOF.

The median calibration coefficients for M13 low gain are also listed in Tables 7 and 8. In addition, the M13 low gain coefficients are plotted versus detector in Figure 7. Note that  $a_0$  exhibits large variations around zero. Also, the gain is much lower than the high gain bands ( $a_1 \sim 7.0$ ); this is necessary in order for M13 to access scene temperatures up to  $\sim 634$  K without saturating. Even though the gain is very low, the linear term still dominates ( $a_2 \sim 10^{-7}$ ), indicating that the response is very linear with the input radiance.

### 3.2 Specifications and Sensitivity

Table 9 shows the median NEdT at  $T_{TYP}$  for all the thermal bands along with the associated requirement. All emissive bands and detectors are well below the specification, including M13 low gain. M14 shows the closest margin to the specification (about 35%). Figure 8 shows the NEdT at  $T_{TYP}$  for all high gain bands versus detector (the red dashed line indicates the requirement). In general, the variation with detector is

small. The exceptions are detector 31 in I5, detector 1 in M12, detector 8 in M16A, all of which are OOF. The NEdT is shown as a function of scene temperature over the optimized range in Figure 9. At lower scene temperatures, the NEdT increases. For the LWIR, the NEdT is below 1.0 K, even at the lowest scene temperatures; for the MWIR, the NEdT increases to around 1.0 K for M12 and M13 at 230 K and roughly 3.5 K for I4 at 230 K.

The RRCU is shown in Table 10 for the worst case detector for each band (note that the requirement of 0.001 for all bands is also included). Most bands fail this specification for at least some detectors (the exceptions are M16A and M16B). This requirement does not apply to M13 low gain. In particular, the MWIR bands I4, M12, and M13 exhibit large RRCU (up to 30 times the specification for I4); this is the result of the nonlinearity at low temperatures in their response versus radiance curves. The RRCU for each detector is plotted in Figure 10 along with the requirement indicated by the red dashed line. Note that the LWIR bands (I5 and M14 – M16) are generally close to or below the specification. Even though most bands and detectors fail this specification, the higher level specifications that also depend heavily on the radiometric fitting (which are discussed below) meet their respective requirements. This indicates that this specification is too strict; a waiver has been authorized by the instrument vendor [9].

Table 11 lists the RRNL for the worst case detector for each band along with the associated specification (0.01). All bands pass this requirement; the closest margin is M14 at about 60%. Again, this requirement does not apply to M13 low gain. Figure 11 graphs the RRNL versus detector for all high gain bands (with a red dashed line for the specification). The non-linearity is very consistent over detectors and HAM sides.

The worst case detector ARD for HAM side A is listed in Table 12 for all high gain emissive bands (there is no requirement for M13 low gain). The ARD for the I bands has a specified limit of 5.0 % (2.5 %) for I4 (I5) at a scene temperature of 267 K. This requirement is assessed at the nearest measured scene temperature, 269.9 K. Both I bands pass the specification with large margins. For the M bands, the requirement is stratified at four scene temperatures for M12 and M13 and five scene temperatures for M14 – M16 (see Table 5). Again, the nearest measured scene temperature to the specified scene temperatures are used to assess the requirement. In all cases, the worst case ARD is well below the specified value (these values are highlighted in green). The worst case detector ARD is graphed in Figure 12 for all bands inside the dynamic range. The ARD for all LWIR bands is less than 0.2 % above 230 K; this indicates that the fitting contribution to the radiance retrieval is very accurate for these bands. In contrast, the MWIR bands I4, M12, and M13 have an ARD of between 0.3 and 0.7 % above a scene temperature of 270 K; below 270 K, the MWIR ARD tend to increase dramatically. The MWIR bands are known to exhibit non-linear behavior, especially below 270 K; the behavior observed in the ARD is the result of fitting residual error in the calibration coefficients. In addition, the MWIR bands are consistently offset by about 0.3 %; this results from the scan by scan OBC correction in the retrieved radiance [see Eq. (9)].

Table 13 lists the RRU for the worst case detector for all high gain thermal bands. This specification applies only between the specified  $L_{MIN}$  and  $0.9L_{MAX}$ ; those scene temperatures outside this range have been grayed out. All high gain bands meet this requirement with the exception of M14 at high scene temperatures; the requirement is met if the RRU is less than 1.0. The RRU generally increases with scene temperature, especially for bands M12, M13 high gain, M14, and M15. The RRU is essentially a measure of detector to detector uniformity in the retrieved radiance in relation to the NEdL, which is an indicator of whether the striping is within the noise resolution. Figure 13 shows the worst case detector RRU for all high gain bands within the optimized dynamic range. The RRU is greater than one for M14 above 327 K; in addition, M13 and M15 approach a RRU of one at high scene temperatures.

In general, the specifications listed in Table 3 do not apply to M13 low gain (with the exception of SRV0053). However, the quantities associated with these specifications (NEdT at  $T_{TYP}$ , RRNL, RRCU, ARD, and RRU) were calculated for M13 low gain as well. The NEdT at  $T_{TYP}$  for M13 low gain is shown in Figure 14; all detectors are well below the specification. The RRCU is below about 0.003 (see Figure 15) and the RRNL is below 0.001 (see Figure 16); the dashed red lines are the specifications for M13 high gain. This indicates that M13 low gain is very linear in its response and that the fitting residual is not large. In addition, the worst case retrieval error (ARD) is less than ~0.5 % at the low end of the dynamic range and less than 0.2 % above 450 K (see Figure 17). In Figure 18, the worst case detector uniformity is well below the detector resolution over the optimized dynamic range. Note that the radiance retrieval is compared to the at-aperture radiance.

#### 4. Summary

- Potential noise contamination at the low end of the specified dynamic range in I4 and M14.
- The linear coefficient  $a_1$  dominates the relationship between radiance and response.
- The  $a_0$  coefficient is small (on the order of  $10^{-2}$  or less).
- The  $a_2$  coefficient is also small (on the order of  $10^{-7}$  or less). The curvature of the MWIR bands is negative, while the curvature of the LWIR bands is positive.
- The NEdT at  $T_{TYP}$  is within the specified resolution for all bands and detectors.
- The nonlinearity is compliant with the specification for all bands and detectors (less than 1 % of the response at  $T_{MAX}$ ).
- The characterization uncertainty is non-compliant for most bands and detectors. However, as the higher level specifications that also depend heavily on the fitting (ARD and RRU) are compliant with their respective specifications, it is believed that this requirement is too strict and hence not representative of the true performance of the sensor.
- The retrieved radiance is within the specified accuracy at all specified scene temperatures.

- Detector to detector striping is within the noise resolution for all bands and detectors over the specified range, with the exception of M14 at high scene temperatures.

## Acknowledgement

The sensor test data used in this document was provided by the Raytheon El Segundo testing team. Approaches for data acquisition and data reductions, as well as data extraction tools were also provided by the Raytheon El Segundo team. We would like to thank the Raytheon El Segundo team for their support. The data analysis tools were developed by the NICST team.

Table 1: F1 RC-05 Part 1 BCS data (Nominal plateau)

UAID	Collect	Gain Mode	BCS Temperature (K)	OBC Temperature (K)
U3103773	2	High	190.0	292.6
U3103773	4	High	210.3	292.7
U3103773	6	High	330.3	292.7
U3103773	8	High	240.2	292.7
U3103773	10	High	247.1	292.7
U3103773	12	High	255.4	292.7
U3103773	14	High	261.8	292.7
U3103773	16	High	269.9	292.7
U3103773	18	High	278.2	292.7
U3103773	21	High	285.3	292.7
U3103773	23	High	292.2	292.7
U3103773	25	High	300.2	292.7
U3103773	27	High	307.2	292.7
U3103773	29	High	315.3	292.7
U3103773	31	High	321.3	292.7
U3103773	33	High	327.3	292.7
U3103773	35	High	332.3	292.7
U3103773	37	High	336.3	292.7
U3103773	39	High	340.4	292.7
U3104144	41	High	345.3	292.7

Table 2: F1 RC-05 Part 1 TMC data (Nominal plateau)

UAID	Collect	Gain Mode	TMC Temperature (K)
U3103773	1	High	292.4
U3103773	3	High	293.1
U3103773	5	High	293.1
U3103773	7	High	293.1
U3103773	9	High	293.1
U3103773	11	High	293.1
U3103773	13	High	293.1
U3103773	15	High	293.1
U3103773	17	High	293.1
U3103773	19	High	293.1
U3103773	22	High	305.1
U3103773	24	High	316.1
U3103773	26	High	325.1
U3103773	28	High	336.1
U3103773	30	High	344.1
U3103773	32	High	351.1
U3103773	34	High	358.1
U3103773	36	High	363.1
U3103773	38	High	369.1
U3103773	40	High	375.1
U3103775	1	Low	388.2
U3103775	5	Low	539.2
U3103775	8	Low	599.2
U3103775	11	Low	645.2
U3103775	14	Low	677.2
U3103775	17	Low	704.1
U3103775	20	Low	730.2
U3103775	23	Low	763.2

Table 3: Specifications addressed by this work [2]

SRV0053	The VIIRS sensor emissive bands shall meet the sensitivity requirements of TABLE 15. (TABLE 15 is listed as Table 4 in this text.)
SRV0448	The VIIRS sensor response shall be characterized with an uncertainty better than 0.1% (mean of the $\Delta L'$ values plus 1 sigma of the $\Delta L'$ values) for the MWIR and LWIR bands.
SRV0595	The nonlinearity (NL) of all spectral bands within a given state shall be less than 0.01 of the response at $L_{MAX} / T_{MAX}$ .
SRV0545	For the bands specified as moderate resolution and emissive, the absolute radiometric calibration uncertainty of spectral radiance shall be equal to or less than the percentage specified in TABLE 17. (TABLE 17 is listed as Table 5 in this text.)
SRV0546	For the bands specified as imaging and emissive (TABLE 1), given a uniform scene of brightness temperature of 267 K, the calibration uncertainty of spectral radiance shall be as specified in TABLE 18. (TABLE 18 is listed as Table 5 in this text.)
SRV0613	The calibrated output of all channels within a band shall be matched to the band mean output within the NE $\Delta$ L / NE $\Delta$ T (1 sigma) when viewing a uniform scene. The matching condition shall be met between radiance levels from $L_{MIN}$ to 0.9 $L_{MAX}$ .

Table 4: Sensitivity requirements for the emissive bands [2]

Band	Center Wavelength (nm)	Gain Type	Single Gain		Dual Gain			
			$T_{TYP}$	NE $\Delta$ T	High Gain		Low Gain	
			$T_{TYP}$	NE $\Delta$ T	$T_{TYP}$	NE $\Delta$ T	$T_{TYP}$	NE $\Delta$ T
M12	3700	Single	270	0.396	~	~	~	~
M13	4050	Dual	~	~	300	0.107	380	0.423
M14	8550	Single	270	0.091	~	~	~	~
M15	10783	Single	300	0.07	~	~	~	~
M16	12013	Single	300	0.072	~	~	~	~
I4	3740	Single	270	2.5	~	~	~	~
I5	11450	Single	210	1.5	~	~	~	~

Table 5: Absolute radiometric calibration uncertainty of the spectral radiance for the emissive bands [2]

Band	Scene Temperature (K)					
	190	230	267	270	310	340
I4	~	~	5.00%	~	~	~
I5	~	~	2.50%	~	~	~
M12	N/A	7.00%	~	0.70%	0.70%	0.70%
M13	N/A	5.70%	~	0.70%	0.70%	0.70%
M14	12.30%	2.40%	~	0.60%	0.40%	0.50%
M15	2.10%	0.60%	~	0.40%	0.40%	0.40%
M16	1.60%	0.60%	~	0.40%	0.40%	0.40%

Table 6: Specified and optimized dynamic ranges

Band	Specified Range		Optimized Range	
	$T_{MIN}$	$T_{MAX}$	$T_{MIN}$	$T_{MAX}$
I4	210	353	210	353
I5	190	340	190	345
M12	230	353	230	353
M13 HG	230	343	230	345
M13 LG	343	634	355	644
M14	190	336	210	340
M15	190	343	190	345
M16A	190	340	190	345
M16B	190	340	190	345

Table 7: Median coefficients for all thermal bands

Band	HAM A			HAM B		
	$a_0$	$a_1$	$a_2$	$a_0$	$a_1$	$a_2$
I4 SS1	3.76E-04	8.81E-04	-2.50E-09	3.80E-04	8.81E-04	-2.37E-09
I5 SS1	-4.84E-03	5.70E-03	1.65E-08	-6.20E-03	5.71E-03	1.67E-08
M12	-1.44E-04	8.19E-04	-1.41E-09	-1.09E-06	1.44E-03	-2.93E-09
M13 HG	3.16E-04	1.65E-03	-5.19E-09	6.59E-03	3.33E-03	-5.05E-09
M13 LG	-2.40E-02	1.42E-01	-1.23E-07	-2.36E-02	1.42E-01	-1.23E-07
M14	1.63E-02	5.14E-03	6.19E-08	6.65E-03	5.32E-03	3.67E-08
M15	-5.73E-03	5.62E-03	1.73E-08	-5.19E-03	5.32E-03	1.84E-08
M16A	1.04E-03	4.89E-03	2.13E-08	3.74E-04	4.90E-03	2.11E-08
M16B	2.17E-04	4.90E-03	2.10E-08	-3.67E-04	4.91E-03	2.10E-08

Table 8: Median gain for all thermal bands

Band	HAM A	HAM B
I4 SS1	1133.1	1132.4
I5 SS1	173.9	173.3
M12	1193.9	1193.5
M13 HG	604.9	604.6
M13 LG	7.1	7.0
M14	195.3	194.2
M15	175.1	177.0
M16A	203.6	203.2
M16B	203.5	203.1

Table 9: Median NEdT at  $T_{TYP}$  for all thermal bands

Band	HAM A	HAM B	Spec
I4	0.413	0.414	2.5
I5	0.413	0.416	1.5
M12	0.116	0.118	0.396
M13 HG	0.044	0.044	0.107
M13 LG	0.191	0.188	0.423
M14	0.060	0.061	0.091
M15	0.029	0.030	0.070
M16A	0.038	0.038	0.072
M16B	0.038	0.038	0.072

Table 10: RRCU worst case detector for HAM side A

Band	HAM A	HAM B	Spec
I4 SS1	0.2660	0.0278	0.001
I5 SS1	0.0015	0.0014	0.001
M12	0.0048	0.0084	0.001
M13 HG	0.0080	0.0091	0.001
M14	0.0022	0.0023	0.001
M15	0.0019	0.0023	0.001
M16A	0.0006	0.0006	0.001
M16B	0.0007	0.0007	0.001

Table 11: RRNL worst case detector for HAM side A

Band	HAM A	HAM B	Spec
I4 SS1	0.002	0.002	0.01
I5 SS1	0.002	0.002	0.01
M12	0.001	0.001	0.01
M13 HG	0.002	0.002	0.01
M14	0.007	0.008	0.01
M15	0.002	0.002	0.01
M16A	0.003	0.003	0.01
M16B	0.003	0.003	0.01

Table 12: ARD worst case detector for HAM side A

BCS T (K)	I4	I5	M12	M13 HG	M14	M15	M16A	M16B
190.0	292.00	0.48	98.76	88.14	1.72	0.53	0.23	0.25
210.3	51.52	0.16	9.54	18.51	0.51	0.11	0.10	0.10
230.3	11.68	0.11	1.80	3.43	0.18	0.08	0.03	0.04
240.2	5.46	0.13	1.26	1.69	0.10	0.06	0.05	0.02
247.1	2.79	0.06	0.88	1.10	0.06	0.08	0.04	0.04
255.4	1.84	0.04	0.71	1.03	0.07	0.07	0.04	0.04
261.8	1.12	0.11	0.58	0.68	0.06	0.07	0.04	0.03
269.9	0.58	0.05	0.33	0.45	0.04	0.05	0.02	0.02
278.2	0.36	0.04	0.27	0.37	0.05	0.04	0.02	0.03
285.3	0.41	0.09	0.32	0.29	0.06	0.04	0.02	0.02
292.2	0.33	0.04	0.32	0.31	0.05	0.04	0.01	0.02
300.2	0.45	0.04	0.30	0.34	0.08	0.03	0.03	0.03
307.2	0.51	0.05	0.31	0.38	0.09	0.02	0.02	0.03
315.3	0.60	0.03	0.30	0.44	0.11	0.02	0.02	0.03
321.3	0.63	0.05	0.28	0.46	0.10	0.02	0.03	0.03
327.3	0.74	0.04	0.34	0.47	0.09	0.03	0.02	0.03
332.3	0.79	0.05	0.33	0.46	0.09	0.03	0.02	0.03
336.3	0.68	0.06	0.31	0.46	0.08	0.04	0.02	0.02
340.4	0.70	0.06	0.31	0.39	0.06	0.04	0.02	0.01
345.3	0.61	0.04	0.31	0.43	0.05	0.04	0.02	0.02

Table 13: RRU worst case detector for HAM side A

BCS T (K)	I4	I5	M12	M13 HG	M14	M15	M16A	M16B
190.0	0.08	0.30	0.09	1.15	0.88	0.40	0.14	0.20
210.3	0.20	0.10	0.30	0.43	0.17	0.24	0.18	0.18
230.3	0.19	0.13	0.16	0.23	0.22	0.29	0.16	0.25
240.2	0.17	0.15	0.23	0.21	0.25	0.18	0.20	0.16
247.1	0.12	0.11	0.23	0.15	0.27	0.39	0.18	0.28
255.4	0.15	0.12	0.11	0.25	0.37	0.48	0.27	0.26
261.8	0.10	0.21	0.17	0.09	0.31	0.45	0.25	0.30
269.9	0.10	0.12	0.12	0.22	0.25	0.42	0.24	0.29
278.2	0.07	0.14	0.13	0.19	0.44	0.36	0.28	0.47
285.3	0.08	0.25	0.16	0.11	0.57	0.41	0.21	0.30
292.2	0.07	0.13	0.08	0.27	0.52	0.67	0.23	0.36
300.2	0.09	0.17	0.22	0.29	0.66	0.66	0.21	0.32
307.2	0.15	0.30	0.24	0.29	0.70	0.49	0.30	0.29
315.3	0.24	0.18	0.27	0.42	0.93	0.64	0.25	0.27
321.3	0.41	0.27	0.30	0.47	0.86	0.62	0.50	0.38
327.3	0.51	0.24	0.61	0.56	1.10	0.93	0.50	0.45
332.3	0.67	0.25	0.63	0.74	1.23	0.72	0.40	0.59
336.3	0.69	0.35	0.64	0.90	1.23	0.77	0.46	0.71
340.4	0.72	0.36	0.73	0.65	1.03	0.94	0.41	0.37
345.3	0.54	0.25	0.68	0.83	1.25	0.97	0.53	0.52

Figure 1: Dynamic range for high gain bands

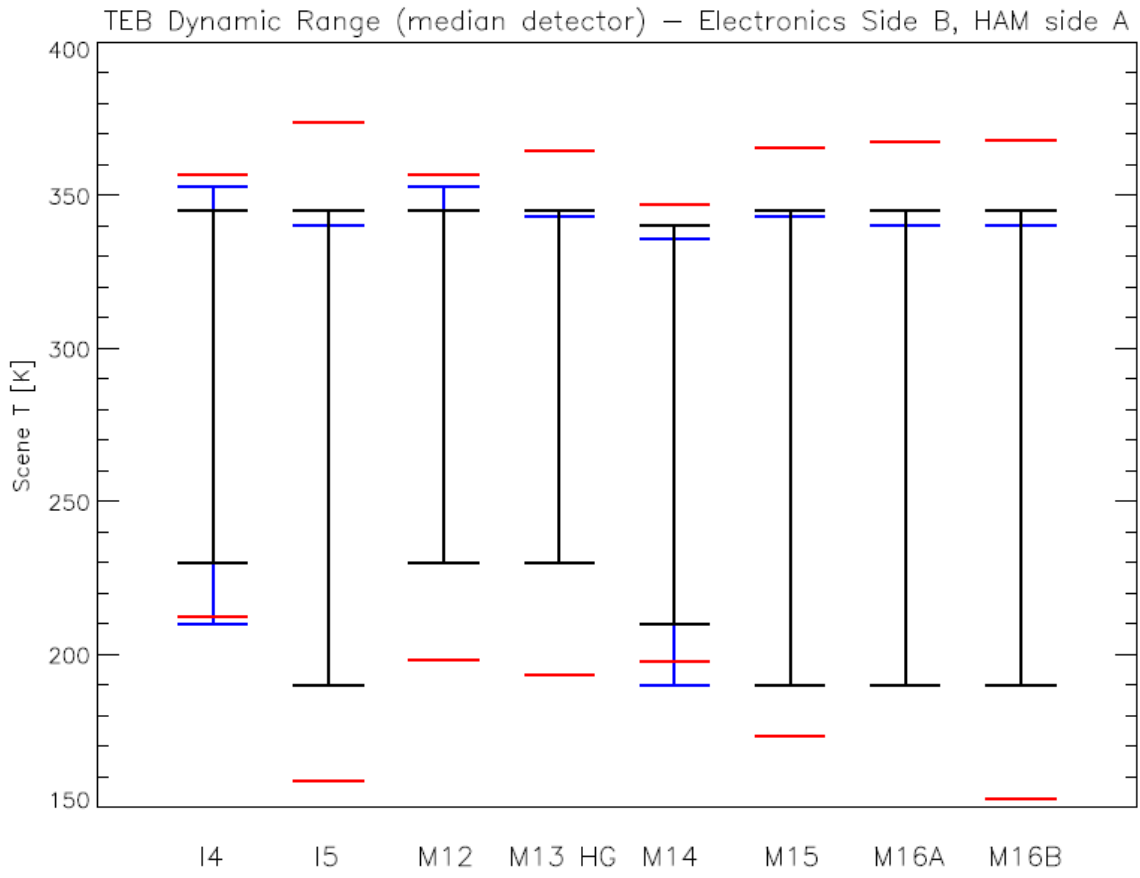


Figure 2:  $\Delta L_{\text{BCS}}$  versus  $dn$  for all high gain bands

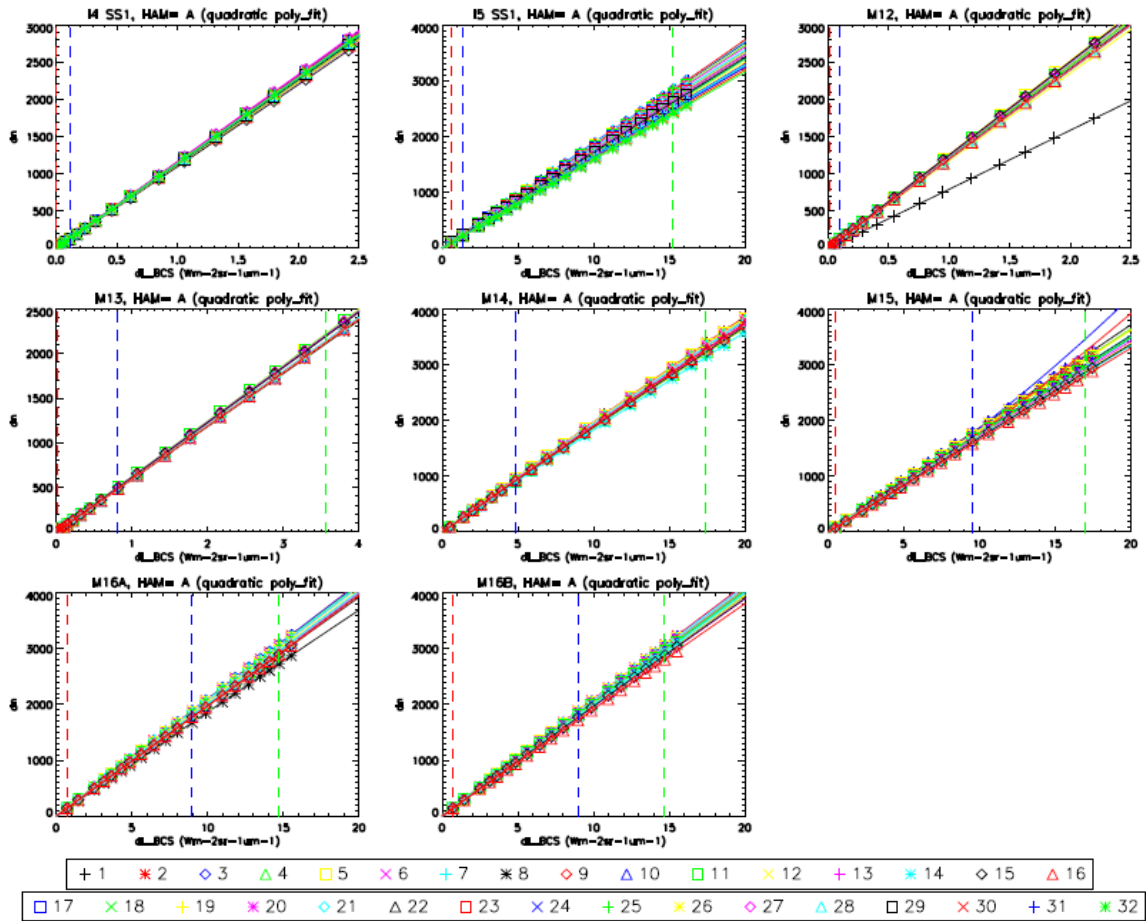


Figure 3: radiance residual for all high gain bands

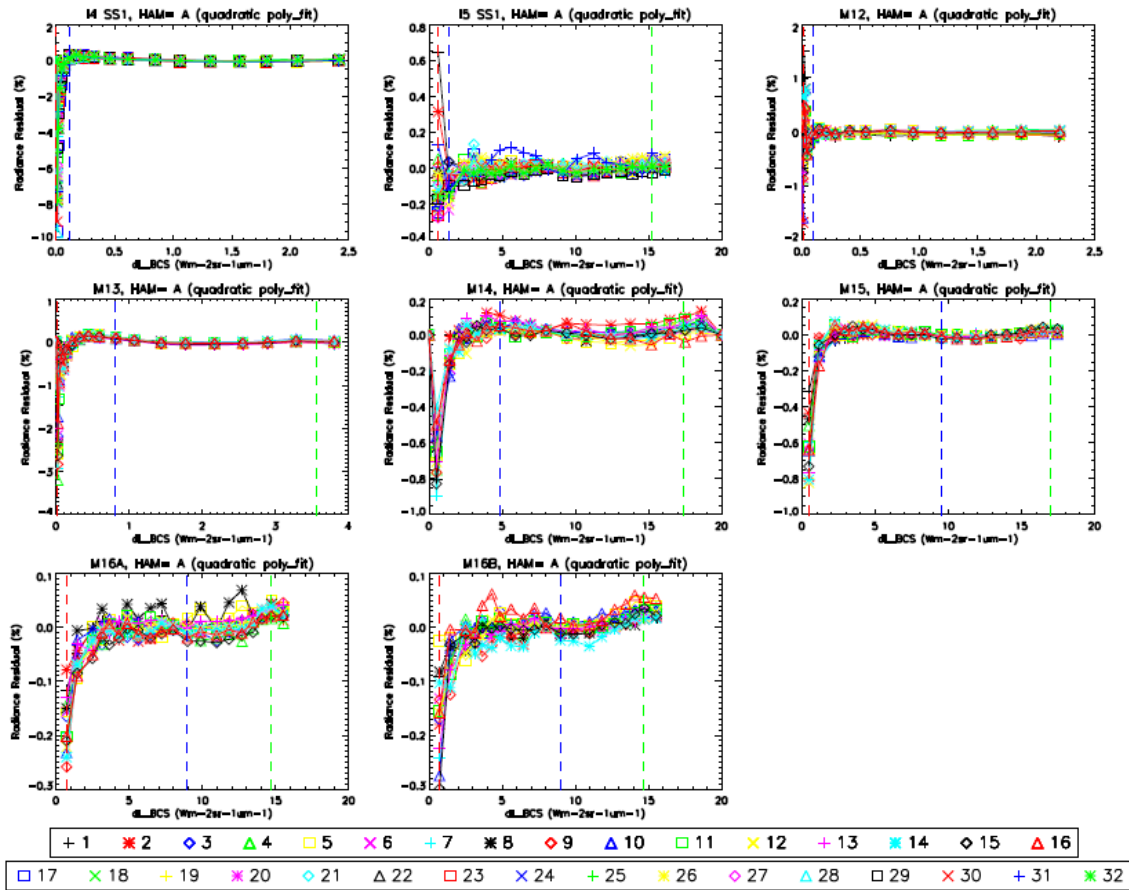


Figure 4:  $a_0$  coefficient for high gain bands

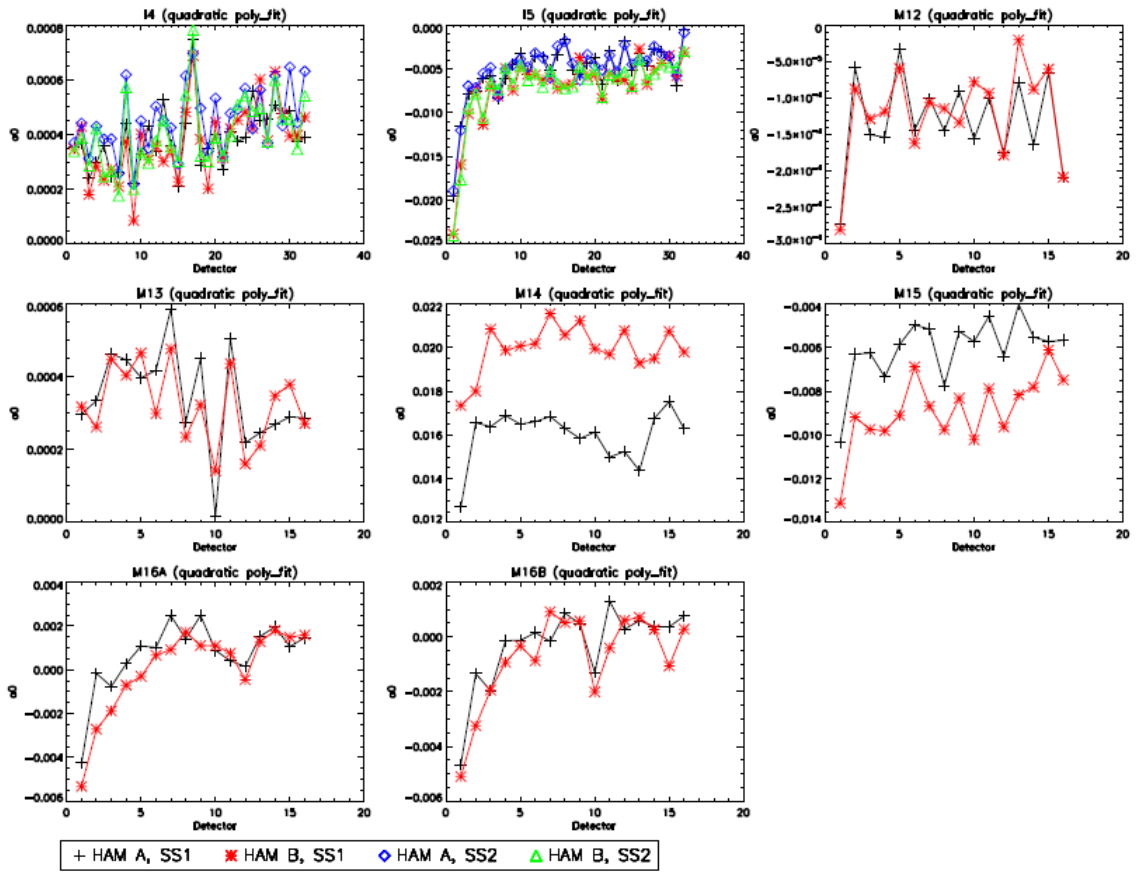


Figure 5: gain ( $1/a_1$ ) for high gain bands

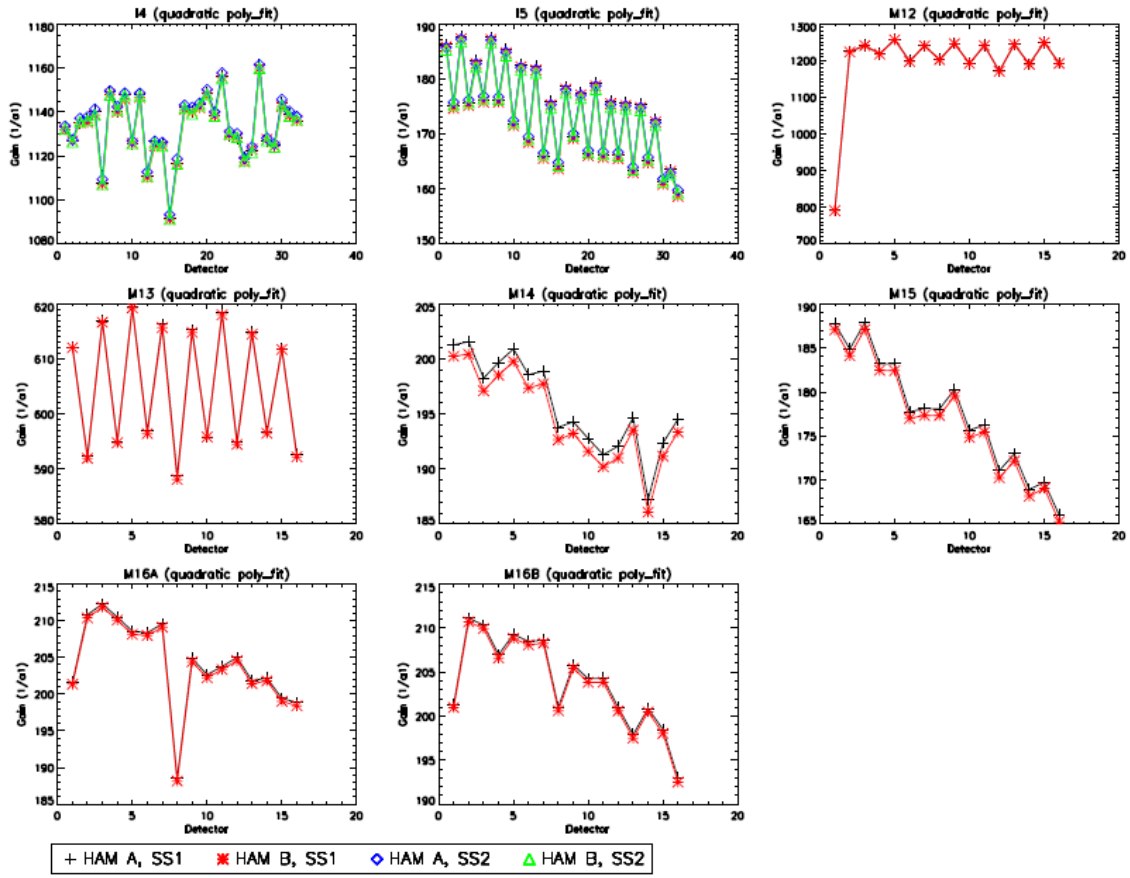


Figure 6:  $a_2$  coefficient for high gain bands

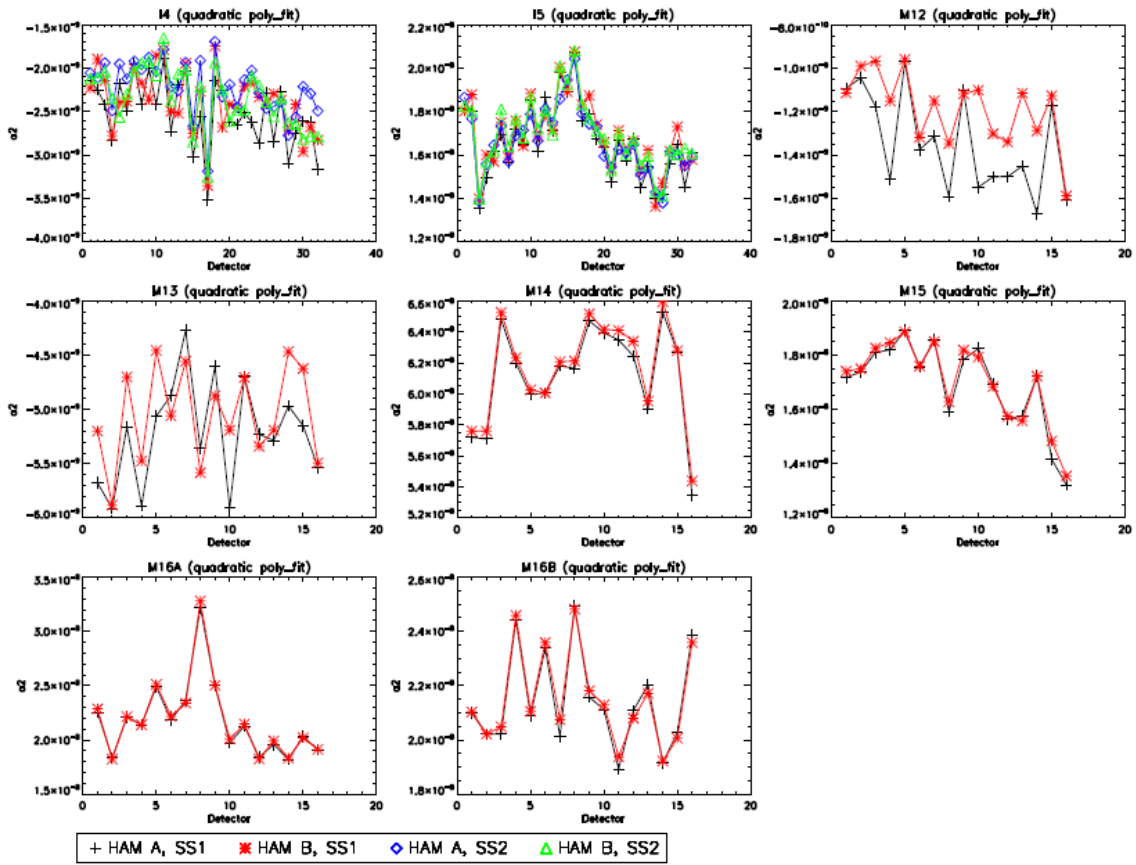


Figure 7: M13 low gain coefficients

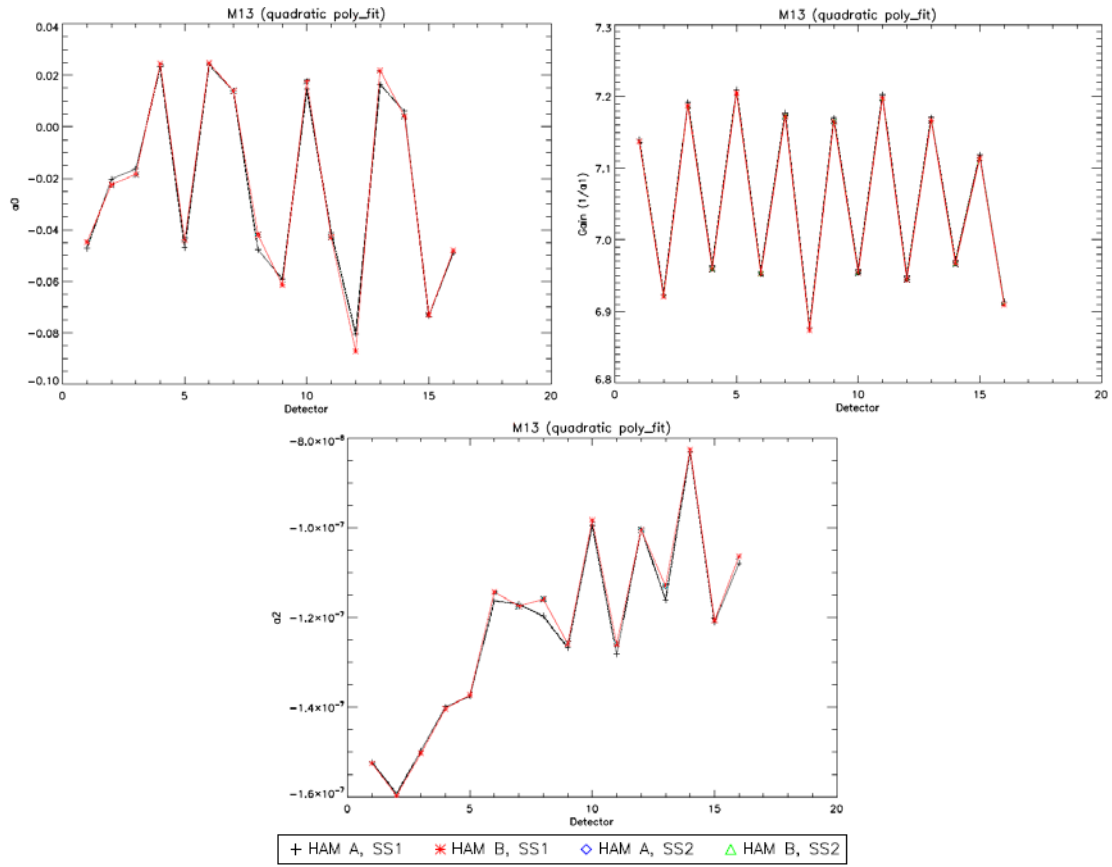


Figure 8: NEDT at  $T_{\text{TYP}}$  for high gain bands

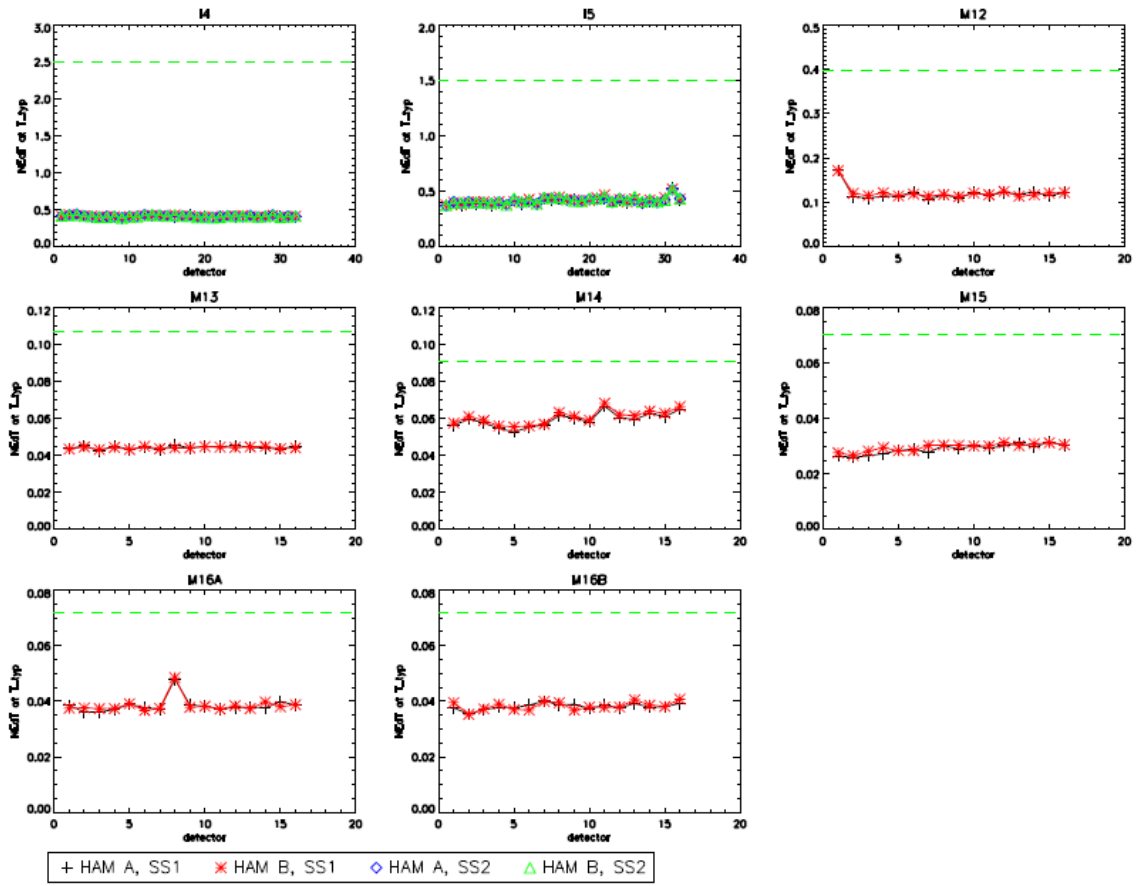


Figure 9: NEdT for high gain bands

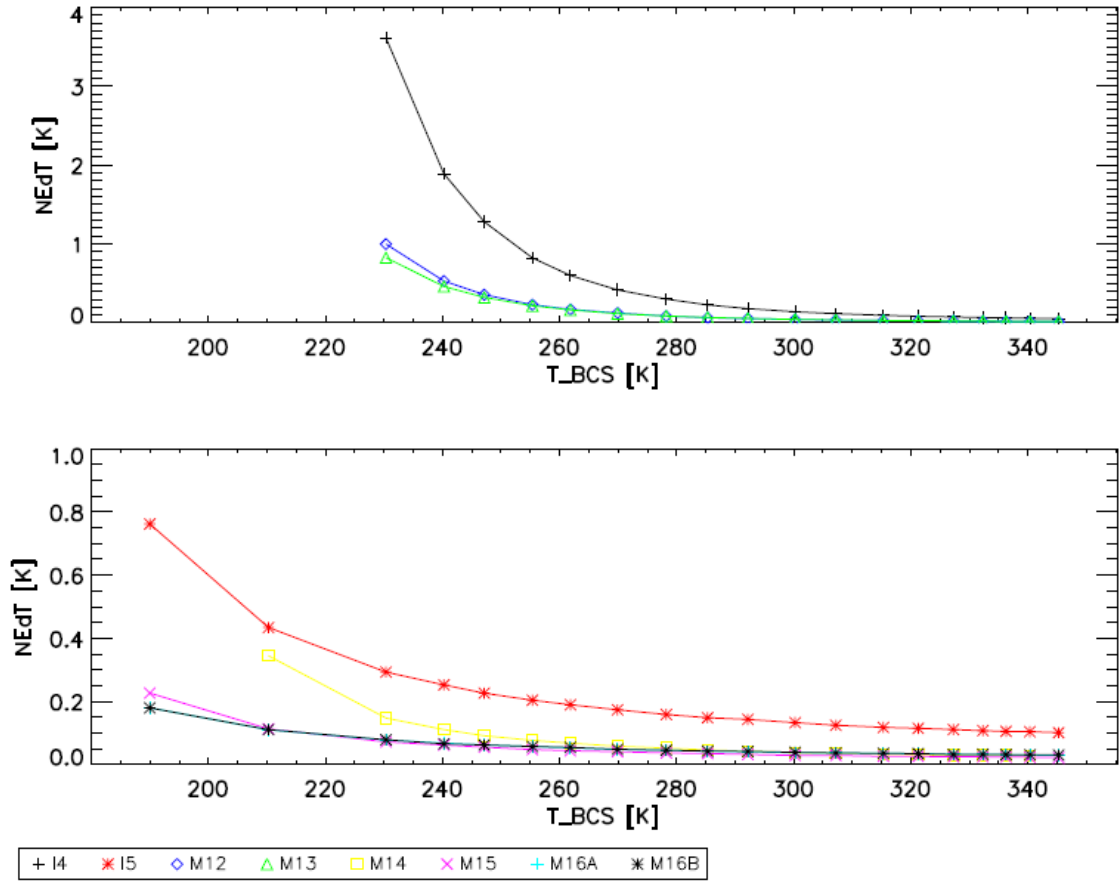


Figure 10: RRCU for high gain bands

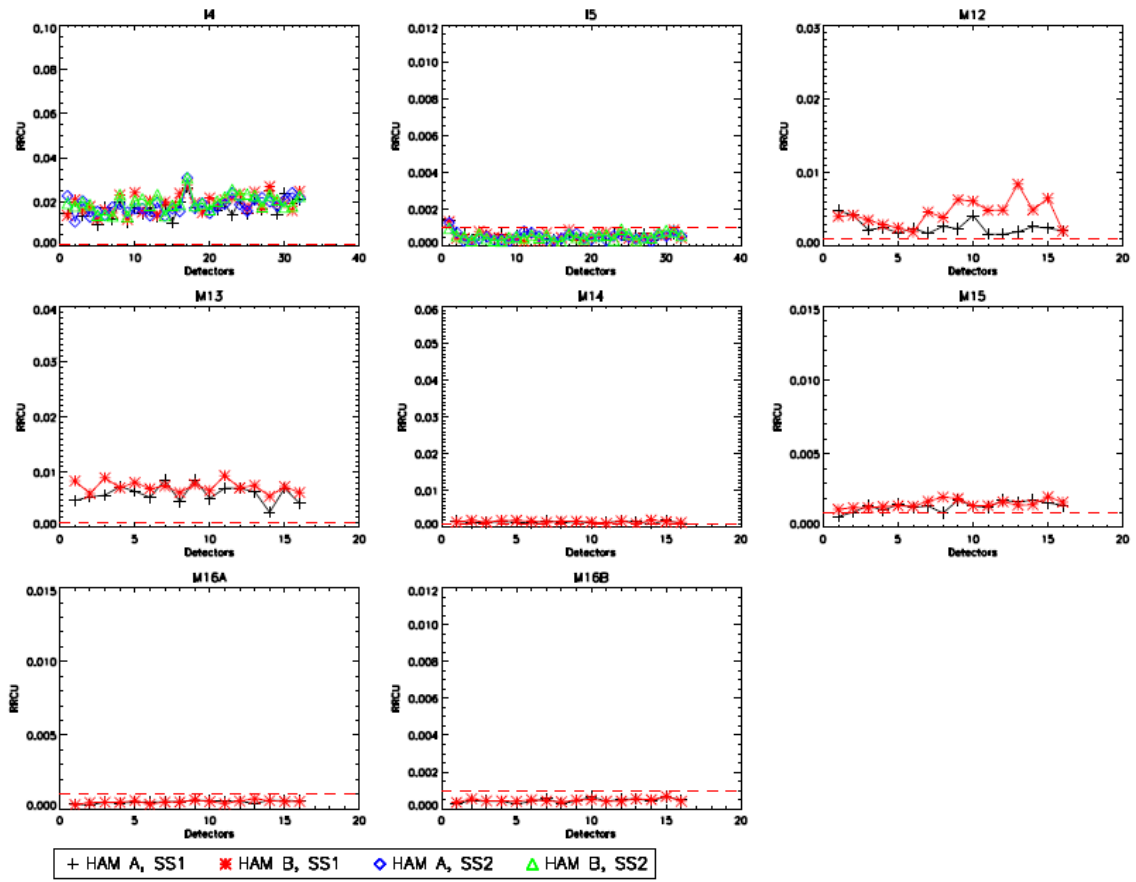


Figure 11: RRNL for high gain bands

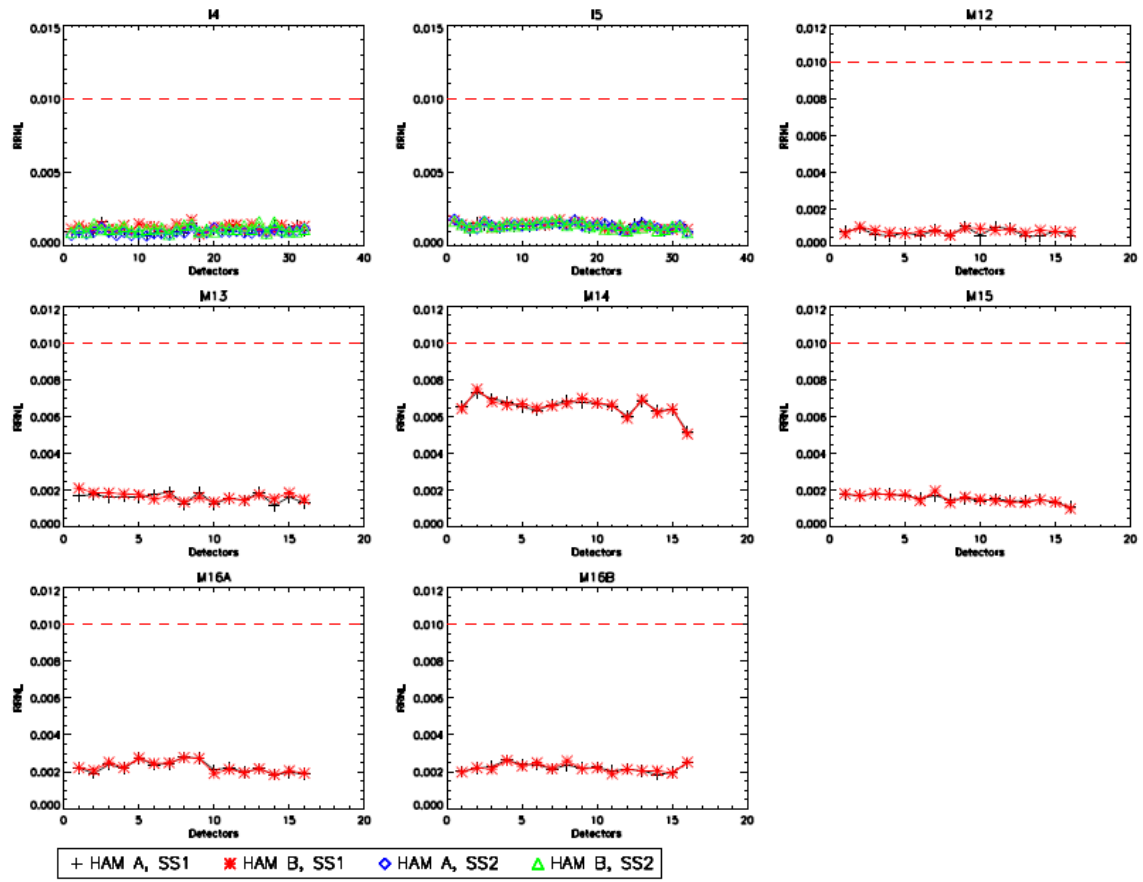


Figure 12: ARD for high gain bands

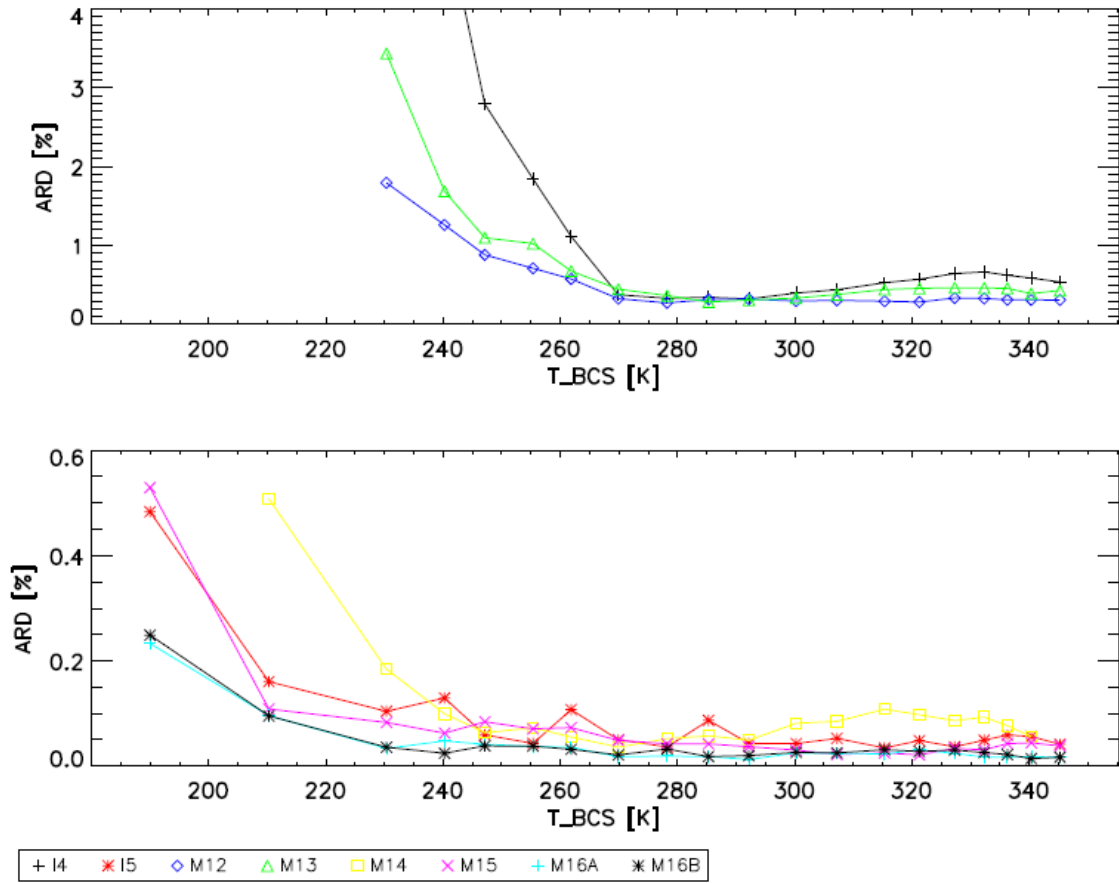


Figure 13: RRU for high gain bands

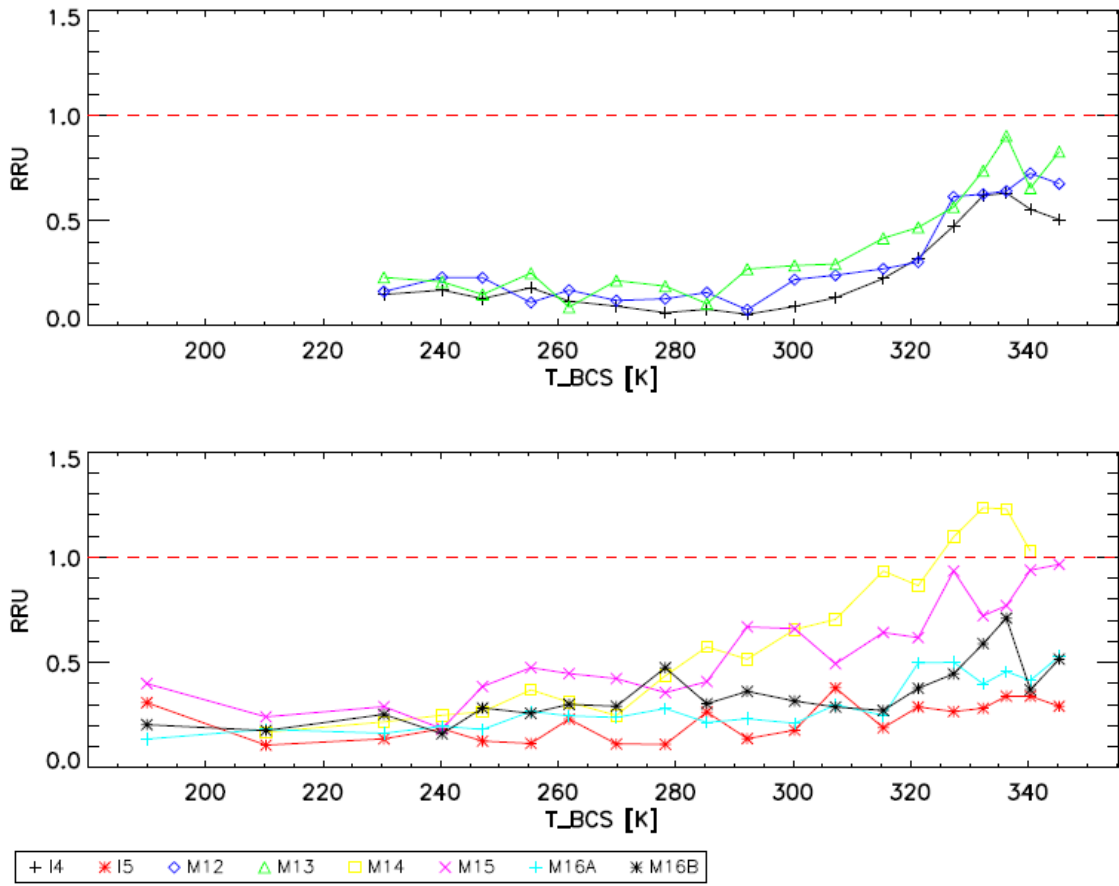


Figure 14: NEdT at  $T_{TYP}$  for M13 low gain

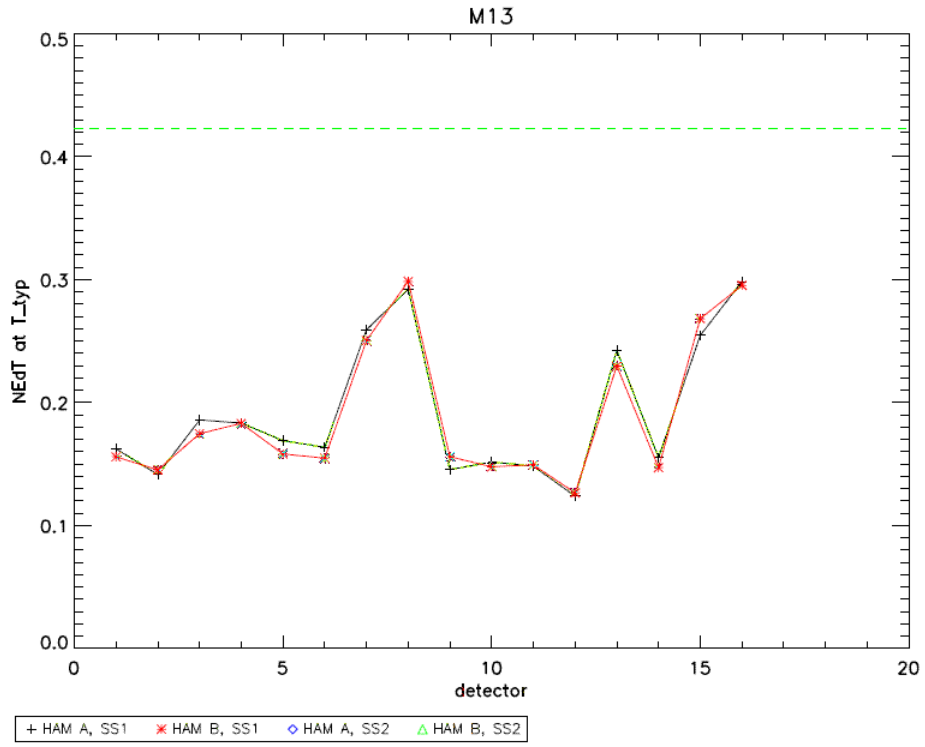


Figure 15: M13 low gain RRCU

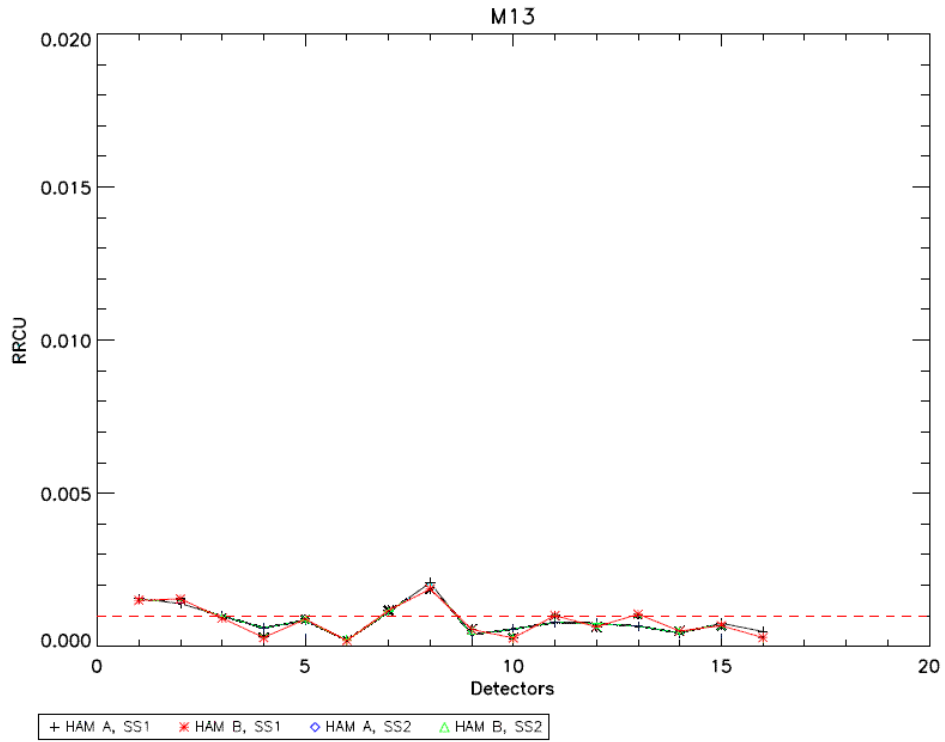


Figure 16: RRNL for M13 low gain

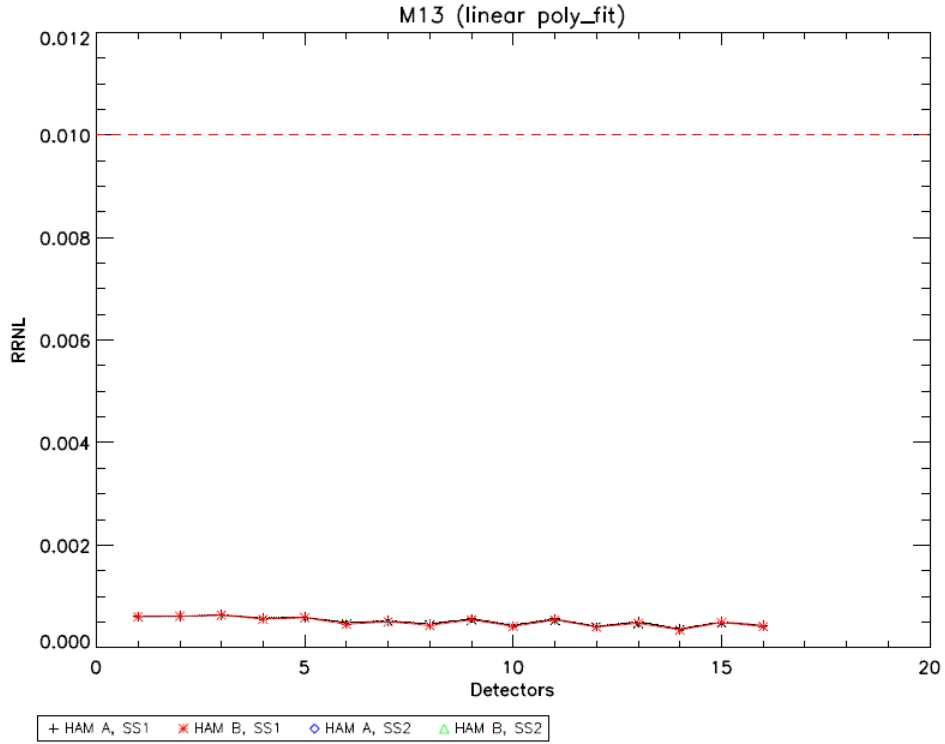


Figure 17: M13 low gain ARD

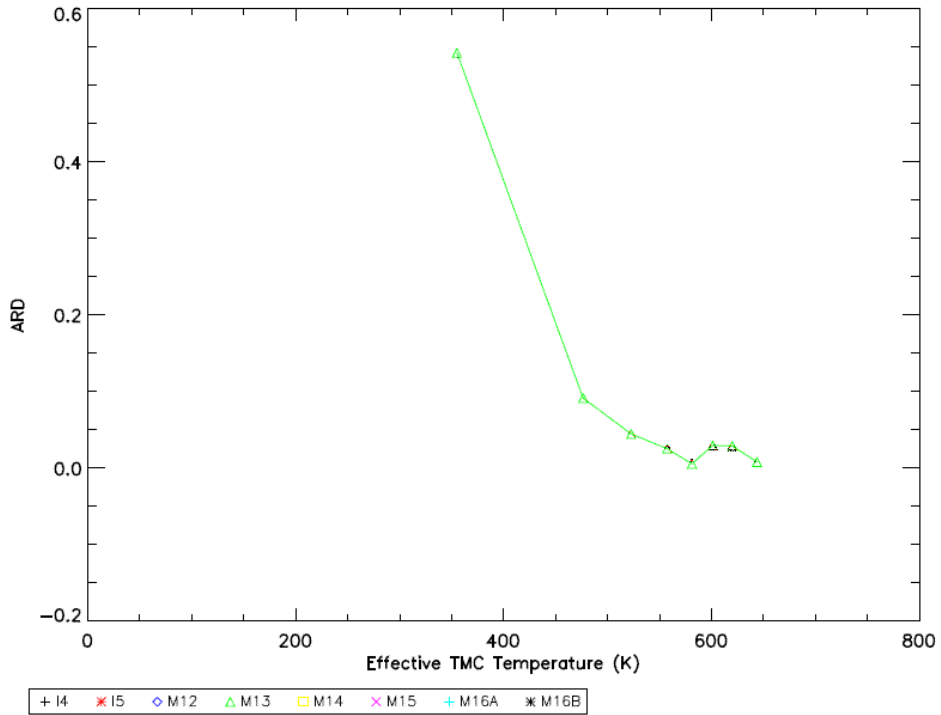


Figure 18: M13 low gain RRU

